# A microfluidic approach to fabricate sucrose decorated liposomes with increased uptake in breast cancer cells

Shiva Khorshid[1], Mariele Montanari[1], Serena Benedetti[1], Sofia Moroni[1], Annalisa Aluigi[1], Barbara Canonico[1], Stefano Papa[1], Mattia Tiboni[1]* and Luca Casettari[1]

[1]*Department of Biomolecular Sciences, University of Urbino Carlo Bo, Piazza del Rinascimento, 6, 61029 Urbino (PU), Italy.*

* Corresponding author: mattia.tiboni@uniurb.it; Tel. (Italy): +390722303336

## Abstract

Nanocarriers are known to control the non-selective activity of conventional chemotherapies that is still a major limitation in the fight against cancer. Developing a targeted drug delivery system is an urgent need to decrease the side effects and increase the drug's efficiency. Most cancer cells show an increased sugar consumption compared to healthy cells due to the deregulation of sugar transporters. Consequently, liposomes, as a biocompatible nanocarrier, could be surface decorated by sugars to enhance drug targeting into cancer cells. Our work outlines a new strategy to easily manufacture sucrose decorated liposomes using sucrose stearate, a biocompatible and biodegradable non-ionic surfactant, with a scalable microfluidic approach. Sucrose decorated liposomes were loaded with berberine hydrochloride, a well-known phytochemical compound to investigate its effects on triple-negative breast cancer cells (MDA-MB-231). Using the microfluidic manufacturing system, we prepared berberine-loaded liposomes using a mixture of phosphatidylcholine and cholesterol with and without sucrose stearate with a size up to 140 nm and narrow polydispersity. Stability was confirmed for 90 days, and the *in vitro* release profile was evaluated. The formulations showed acceptable *in vitro* biocompatibility and significantly higher anti-proliferative effect on MDA-MB-231 cell line. These results have been confirmed by an increased uptake evaluated by flow cytometry and confocal microscopy. Taken together, our findings represent an innovative, easy, and scalable approach to obtain

sugar decorated liposomal formulations without any surface-chemistry reactions. They can be potentially used as an anticancer targeted drug delivery system.

**Keywords:** Additive manufacturing; 3D printed microfluidic chips; nanomedicine; sucrose esters; Surface modification.

## 1. Introduction

Based on World Health Organization statistics, breast cancers are the most prevalent cancer and the main reason for death in women (1). About 10-20 % of the diagnosed breast cancers are sorted as triple-negative breast cancer (TNBC) which is the most problematic subtype that has no therapeutic target due to estrogen (ER), progesterone (PR), and HER2 protein lack of expression (2). A major drawback for cancer therapy is the non-selectivity of conventional therapies which cause adverse side effects and a significant decrease in drug efficiency (3,4). Therefore, there is an imperative need to investigate new therapeutic agents and targeted drug delivery systems (DDS) to cure invasive breast cancer more efficiently.

Among nano DDS, liposomes are small spherical structures (5) that could be modified with different active targeting agents (6). As a drug delivery system, liposomes have proper bioavailability, size controlling measures, long half-lives, control release features, low risk to benefit ratio (5), self-assembly potential, and the ability to protect drugs to have long-lasting activation (7). Thin-film hydration, ethanol injection, and proliposome-liposome method are the conventional ways to develop liposomes (8). With all these methods developing a proper liposome encounter some challenges, such as high dispersed particles, batch to batch variability, time-consuming preparation, and non-reproducible formulations (8,9).

Microfluidics is an innovative, scalable liposome manufacturing method that can overcome these issues by controlling the flow conduction of the fluids through micrometer channels (10,11). These microchannels could have different geometries (12) which can affect the flow and consequently the self-assembly of the nanocarriers (11). In recent years, by the advent of microfluidic technology, which is a simple and automized technique, the physical characteristics of the liposomes could be predictable, tunable, and reproducible by the control of the main microfluidic parameters such as flow rate ratio (FRR) and total flow rate (TFR) (9,13). Subsequently, the microfluidic method allows the preparation of liposomes in a more reproducible and time-saving manner (12) to deliver a precise amount of drugs (14). Furthermore, liposomes have the ability to entrap both hydrophilic and hydrophobic drugs due to the amphiphilic nature (5,7).

Berberine, which has been chosen as a model drug in this work, is an isoquinoline alkaloid bioactive which can be isolated mainly from Barberry (*Berberis vulgaris* L. belongs to the Berberidaceae family) and attracts considerable interest due to its pharmacological effects. Investigations on berberine are

mostly on its anti-inflammatory (15–18), and anti-microbial properties (19–21). Moreover, there are some *in vitro* and *in vivo* investigations on berberine's effect on different cancer cell lines, such as prostatic (22,23), gastrointestinal (24–26), hepatic (27), dermal (28), and breast (27,29). It has been demonstrated that berberine can arrest the G0/G1 cell cycle and induce apoptosis in breast cancer cells with estrogen receptors (27) and various cell lines (30). Despite all these characteristics and therapeutic effects of berberine, low solubility (31) and low bioavailability (0.68%), which is probably related to berberine structure as quaternary ammonium (32), are some of the limitations for berberine clinical usage.

In this work, liposomes and sucrose decorated liposomes were prepared using the microfluidic method throughout innovative 3D printed chips with two different microchannel geometries that have been developed previously by our group (33). Liposomes were prepared using soybean phosphatidylcholine (PC), and cholesterol, meanwhile for sucrose decorated liposomes, sucrose stearate was added as a renewable, and functional non-ionic surfactant that allows the presence of a sugar moiety on the surface of the nanocarrier (34). While there is deregulation in cancer cells sugar transporter, they take and consume more sugar than the normal cell lines (35). Pathophysiological and specific molecular characteristics of cancer cells could be exploited to reach targeted DDS (6,36). Different targeting agents such as peptides, folic acid (3,4), antibodies (4), and carbohydrates (3,4,36–39) have been used to facilitate targeted drug delivery in cancer therapies. In spite of the fact that the targeting moieties are usually attached by chemical reactions (4,6) our work insert the sugar moieties on the surface of liposomes with the aim of reaching an active targeting on cancer cells with no surface chemistry steps needed before or after the formulation of the nanocarrier. Modifying nanocarriers with carbohydrate targeting agents could enhance the drug uptake by the cancer cells (3,4) by active and passive mechanisms (6). The integration of sucrose ester could enhance the drug efficacy on cancer cells growth inhibition by increasing the nanovesicles uptake by cancer cells. The colloidal systems were characterized by their average particle size, polydispersity index (PDI), and encapsulation efficiency (EE%). The characteristics of optimized liposomes were evaluated by Fourier-transformed infrared spectroscopy (FTIR), and thermogravimetric analysis (TGA). Cytocompatibility of the loaded and unloaded liposomes was performed on AC16 cardiomyocyte cells by Sulforhodamine B (SRB) assay. Moreover, the antiproliferative effects of the mentioned formulations were tested to confirm the effect of liposome to increase berberine's bioavailability and the sucrose ester effects on enhancing

liposome's antiproliferative effectivity. Cell uptake of the different formulations prepared was evaluated by flow cytometry coupled with confocal microscopy.

## 2. Materials and methods

### *2.1. Materials and cell lines*

Berberine hydrochloride (BBH) was purchased from A.C.E.F. (Italy), sucrose stearate (SS) was obtained from Chem Service (USA), cholesterol (Chol) was kindly obtained from CRODA (UK). soybean phosphatidylcholine (PC) (soybean lecithin, 94% of phosphatidylcholine) was kindly provided by Lipoid (Germany). Polypropylene (PP) was kindly gifted from BASF (Germany). All the other solvents used were analytical grade.

### *2.2. 3D printing of microfluidic chips*

The 3D printed chips were designed and printed as described before (9). Briefly, the design of the microfluidic chip was optimized using a computer-aided design (CAD) to obtain an effective passive micromixing with a "zigzag" bas-relief (Z-chip) and "split and recombine" channels (C-chip). Thereafter, the chips were printed using polypropylene with a fused deposition modeling (FDM) 3D printer (Ultimaker 3, Ultimaker, The Netherlands) at a print speed of 25 mm/s and with a nozzle temperature of 220 °C (0.25 mm nozzle). This allowed obtaining leak-free and semi-transparent devices. Probe needles were used to connect the chip to syringe pumps (Aladdin, WPI Europe, Germany) through PTFE tubing.

### *2.3. Preparations of the liposomes by the microfluidic method*

For the preparation of normal liposome (NL) by the microfluidic method, a total concentration of 8 mg/mL of PC, and Chol with the weight ratio of 3:1 was dissolved in the ethanolic phase. Thereafter, the 3D printed chips were connected through PTFE tubing to two syringes, containing water and ethanolic phase, that were settled on syringe pumps to control the flow. The ethanolic and water phases were mixed with FRR (water/ethanol) of 2:1 and TFR 8 mL/min. Finally, the flow-out liposomes were collected from the chip's outlet. The ethanol in the final formulation was discharged with one round of centrifuge at 17200 RCF for 60 min at 4 °C. Thereafter, the pellets were resuspended in water to reach

the primary concentration. In order to prepare sucrose decorated liposomes (SL), the total concentration of 8 mg/mL of SS, PC, and Chol with the weight ratio of 3:1:1 and 3:1:2 was dissolved in the ethanolic phase. The rest of the process is as for normal liposomes with FRR 2:1 and different TFR (8, 10, 12, and 14 mL/min). To obtain BBH loaded liposomes BBH@NL and BBH@SL, 3 mg/mL of BBH were previously dissolved in the water phase at 60 °C and then mixed through the microfluidic device with the other excipients contained in the ethanolic phase.

### *2.4. Characterization of colloidal systems*

Physical characteristics of the formulation were investigated by measuring the average particle size (Z-average) and polydispersity index (PDI) using Malvern Zetasizer Nano S instrument (Malvern Instrument Ltd, UK). Prior to the measurements, the formulations were diluted at 1:10 in distilled water. For further characterization, attenuated total reflectance Fourier-transformed infrared spectroscopy (ATR-FTIR, Spectrum Two FT-IR spectrometer with ATR accessory, Perkin Elmer, MA, USA) were operated at 400–4000 $cm^{-1}$ to evaluate the interaction between BBH, SS, Chol, PC, SL, BBH@SL, NL, BBH@NL. The FTIR test was performed on freeze-dried liposomes.

Moreover, thermo-gravimetric analysis (TGA) was used to investigate the thermal behavior of the component based on their weight loss with increasing temperature. TGA was performed using a TGA 4000 (PerkinElmer, Norwalk, USA) equipped with an intercooler (Intracooler 2, PerkinElmer, Norwalk, USA) in an inert nitrogen atmosphere. Chol+PC (NL), Chol+PC+BBH (BBH@NL), Chol+PC+SS (SL), Chol+PC+SS+BBH (BBH@SL) were analyzed in the temperature range of 30 to 500 °C with the heating rate of 20 °C/min and 10 °C/min from 30 to 80° C and 80 to 500° C, respectively, under nitrogen atmosphere with the gas flow of 30 mL/min.

### *2.5. Quantitative determination of berberine by HPLC*

The amount of BBH in the experiments performed was evaluated by high-performance liquid chromatography (HPLC Agilent 1260 Infinity II, Agilent, USA). The mobile phase was a mixture of water and acetonitrile (65:35 v/v) with 0.05 % of Trifluoroacetic acid (TFA) at a flow rate of 1 mL/min.

151 The injection volume was 20 µL in the column EC-C18, 100 × 4.6 mm, 2.7 µm column (Agilent, USA)
152 monitored at 345 nm.

153

154 *2.6. Encapsulation efficiency studies*

155 Encapsulation efficiency (EE%) studies were assessed by direct method. Firstly, a calibration curve of
156 BBH was performed with five concentrations in the range of 0.001 to 0.01 mg/mL with a coefficient
157 of determination ($R^2$) of 0.9986. The collected liposomes from the chip were centrifuged at 17200 RCF
158 at 4° C for 60 min to settle the drug-containing liposomes. The supernatant was discharged to remove
159 unloaded BBH and ethanol. Subsequently, 1 mL of methanol was added to dissolve the liposome
160 structure and extract the encapsulated BBH. Then, the amount of loaded BBH was measured by HPLC.

161 Accordingly, the encapsulation efficiency (EE%) of the microfluidic liposome was calculated with the
162 following formula through the direct method.

163 $EE\% = (E_{drug}/T_{drug}) \times 100$

164 In the above formulation, $E_{drug}$ is referred to the encapsulated amount of drug measured by the HPLC
165 and $T_{drug}$ is the total amount of used drug in the primary formulation.

166

167 *2.7. Stability test*

168 The stability of the optimized formulation was evaluated at 4 and 25 °C for up to 90 days in terms of
169 size, PDI, and EE%. The measurements have been performed after 7, 14, 30, 60 and 90 days.

170

171 *2.8. Release studies*

172 *2.8.1. In vitro release of berberine hydrochloride from liposomes*

173 The release of BBH from NL and SL was investigated in phosphate-buffered saline (PBS pH 7.4) and
174 acetate buffer (pH 5.5) to simulate physiologic and cancerous cells pH (40), respectively. Briefly, 1 mL
175 of the BBH loaded liposomes (BBH@NL and BBH@SL) and free BBH at a concentration equal to the
176 BBH encapsulated into the liposome were placed in a dialysis bag (MW cut off 12k-14k Da,

Spectra/Por™, Spectrum Labs, USA) and immersed into 50 mL of PBS and acetate buffer continuously stirred at 100 rpm keeping the system at 37 °C. At each time point (0.25, 0.5, 1, 2, 3, 4, and 6 h), 1 mL of the medium was collected and replaced with the same amount of fresh release medium. The BBH concentrations were measured with HPLC.

*2.8.2. Mathematical Modeling of the Kinetics Release*

The drug release data of the samples were modeled using the first-order, Higuchi, and Peppas-Salhin mathematical models using Origin Software (Origin Pro 2021, OriginLab, USA). The adjusted coefficient of determination (adjusted-$R^2$) was used to select the best-fitting model.

*2.9. In vitro cytocompatibility on Human Cardiomyocyte Cell Line (AC16)*

The human cardiomyocyte cell line AC16 was grown in Gibco Dulbecco's Modified Eagle Medium: Nutrient Mixture F-12 (DMEM/F-12) supplemented with 12.5 % FBS, 1 % penicillin/streptomycin 100 U/mL, and 2 mM L-glutamine. Cells were maintained in T25 flasks in a $CO_2$ incubator at 37 °C and 5 % $CO_2$. Cytocompatibility of different formulations with and without SS and BBH (BBH@SL, SL, BBH@NL, NL) was studied by Sulforhodamine B (SRB) assays by evaluating the cell protein content. AC16 ($4x10^3$ cells/well) were seeded in 96-well plates and treated with: a) NL 125, 250, 500 µg/mL; b) SL 125, 250, 500 µg/mL; c) free BBH 3, 6, 12 µg/mL (corresponding to the amount of encapsulated BBH in the nanocarriers); d) BBH@NL 125, 250, 500 µg/mL; and e) BBH@SL 125, 250, 500 µg/ml. After 24 h of incubation, test compounds were removed, cells were washed with PBS, and then fixed by adding trichloroacetic acid (TCA) 50 % (w/v). The plate was incubated for 1 h at 4 °C and then rinsed with water 3 times. The plate was dried at room temperature and 0.4 % SRB was added to the wells and let the cells match the color for 30 min. Eventually, cells were rinsed with acetic acid 1 % as many times to remove the unincorporated color. To solubilize the incorporated dye, 10mM tris was added and the absorbance was measured at 570 nm in a microplate reader (Multiskan FC, Thermo Scientific) (41). Data were expressed as a percentage (%) versus non-treated cells (controls).

### *2.10. Antiproliferative studies on epithelial, human breast cancer cell line MDA-MB-231*

The human triple-negative breast cancer cell line MDA-MB-231 was grown in DMEM medium supplemented with 10 % FBS, 1 % penicillin/streptomycin 100 U/mL, 2 mM L-glutamine, and 1 % non-essential amino acid solution. Cells were maintained in T25 flasks in a $CO_2$ incubator at 37 °C and 5 % $CO_2$. In order to investigate the advantages of loaded drug compared to the free one, SS effect, and the microfluidic BBH-loaded liposomes on MDA-MB-231 breast cancer cells, different concentrations of NL, SL, BBH@NL, and BBH@SL (125, 250, 500 µg/mL) were seeded in 96-well plates containing $5 \times 10^3$/well MDA-MB-231 cells and incubated for 24 h. Afterward, the cytotoxic effects of the microfluidic liposomes were evaluated by SRB assays as explained before.

### *2.11. Cell uptake studies*

To evaluate NL and SL uptake by MDA-MB-231, BBH-loaded liposomes were labeled with Rhodamine (1% w/w of 18:1 Lyss Rhod PE, Avanti Polar Lipid, USA). The fluorescent lipid was solved in the ethanolic phase together with the other excipients and incorporated during liposome microfluidic assembly.

Cancer cells were seeded in 12-well plates ($1.5x10^5$ cells/well) and treated with rhodamine-labeled NL and SL 250 µg/mL for 4 and 24 h. After the incubation time, liposomes were removed, cells detached by trypsinization, and washed with PBS at 1200 rpm for 10 min.

To label and trace lysosomes, the acidotropic dye LysoTracker Deep Red (LTDR) (Thermo Fisher Scientific, Waltham, MA, USA) was used. The amount of fluorescence obtained from staining with LysoTracker is directly related to the volume of lysosome-related organelles in a cell (42) . Cell pellets were resuspended in 300 µl PBS containing 100 nM of LysoTracker. After 30 min of incubation, red lysosomal fluorescence was detected by flow cytometry and confocal microscopy (43).

CD71 antibody is specific for the human transferrin receptor, which is essential for iron transport into proliferating cells (44); indeed, the presence of iron within the cell is necessary for cell proliferation and is responsible for many cell functions such as DNA synthesis, oxygen sensing, and transitioning from the G1 to the S phase in the cell cycle (45). To evaluate CD71 surface expression, FITC-conjugated anti-CD71 monoclonal antibody (clone L01.1) (BD Biosciences, San Jose CA, USA) was added to 70 µL of cell pellet, at dilutions according to the manufacturer's instructions. After 20 min of incubation at RT, samples were acquired by flow cytometry and confocal microscopy.

To investigate the involvement of sugar receptors in SL uptake, MDA-MB-231 were seeded in 12-well plates ($1.5x10^5$ cells/well) and pre-treated with sucrose 0.75 M for 20 min at 37°C to block sucrose receptors (46) before incubation with rhodamine-labeled SL 250 µg/mL for two different periods (20 min and 40 min).

### *2.12. Cytometric Investigations*

Cytometric experiments were carried out with a FACSCanto II flow cytometer (BD, Franklin, Lakes, NJ, USA) equipped with an argon laser (Blue, Excitation 488 nm), a helium-neon laser (Red, Excitation 633 nm), and a solid-state diode laser (Violet, Ex 405 nm). Analyses were performed with the FACSDivaTM software (BD); 10,000 cell events were acquired for each sample.

### *2.13. Confocal Microscopy*

Confocal microscopy analyses were performed with a Leica TCS SP5 II confocal microscope (Leica Microsystem, Germany) with 488, 543, and 633 nm illuminations and oil-immersed objectives. For confocal live imaging, MatTek glass-bottom chambers (MatTek Corporation, Bratislava, Slovak Republic) were used. The images were further processed and analyzed in ImageJ software (NIH, Bethesda, MD, USA).

### *2.14. Statistical Analysis*

All data were expressed as the mean ± standard deviation (SD) based on at least three tests. Statistical analysis was carried out using Origin software (Origin Pro 2021b). A $P$ value $<0.05$ was considered statistically significant.

## 3. Results and discussion

### *3.1. Microfluidic assembly and characterization of liposomes*

In this study, we prepared a new class of microfluidic assembled liposomes decorated with sucrose to increase the uptake in MDA-MB-231 breast cancer cells. BBH was successfully loaded into this innovative system to formulate liposomes. The sucrose decoration was obtained using sucrose stearate that belongs to the class of sugar esters, non-ionic surfactants that can be effectively used alone or in combination with other lipids to formulate colloidal drug delivery systems (34) The use of these surfactants allows to insert the sugar moieties on the surface of liposomes with the aim of reaching an active targeting on cancer cells with no surface chemistry steps needed before or after the formulation of the nanocarrier. To obtain the optimum ratio of SS, PC, and Chol we characterized the liposomes in terms of size and stability starting from different weight ratios (3:1:1, 3:1:2) and different microfluidic parameters (TFR and FRR) using the 3D printed C-chip and Z-chip (**Fig. 1**). Our results (**Fig. 2**) showed that the 3:1:2 ratio possessed both lower size and higher stability due to increased amount of cholesterol, which can arrange alkyl chains ordering of the lipid and increase membrane density (47), while the liposomes with 3:1:1 ratio were not stable and they showed 40 nm increase in the size after one week. Moreover, different trials with TFR (8, 10, 12, and 14 mL/min) and the two different chips (C and Z-chip) showed smaller sizes using Z-chip and 14 mL/min (**Fig. 2**). Based on the liposome size and stability, the finest TFR and FRR are 14 and 2:1, respectively. The highest concentration of BBH (3 mg/mL) without any precipitation was used and solved in water at 60 °C.

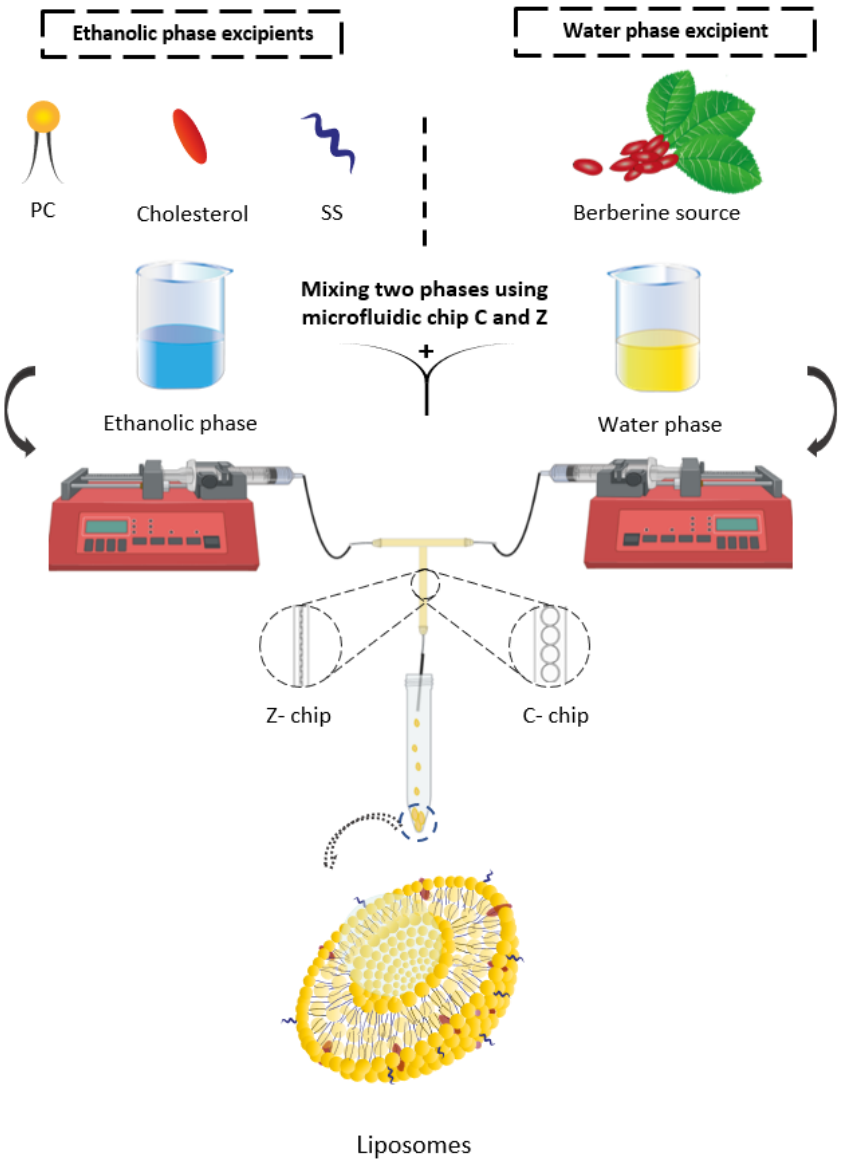


**Fig. 1.** Microfluidic assembly of liposomes

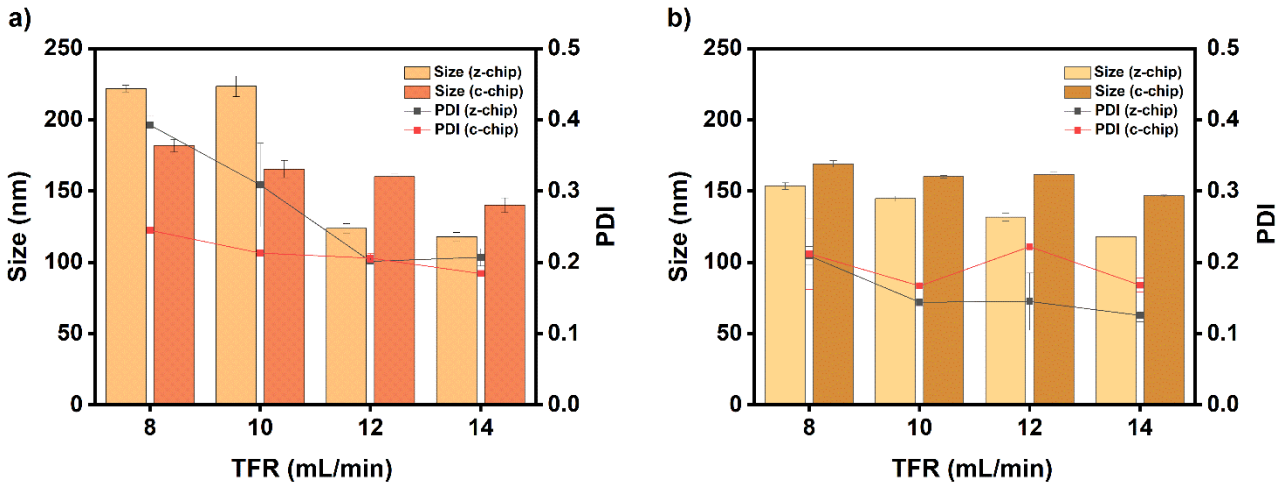


**Fig. 2.** Sucrose decorated liposomes optimization considering different TFR (8, 10, 12, 14 mL/min) and T-shape chips (C-chip and Z-chip) with SS: PC: Chol ratio of a) 3:1:1 b) 3:1:2. Data are reported as the mean of three independent replication of experiments ± SD.

Based on the characterization, we choose the ratio of 3:1:2 of SS:PC:Chol, FRR 2:1 (water: ethanolic phase), and TFR (14 mL/min) for SL, and the ratio of 3:1 of PC:Chol has been chosen for NL. NL shows an average size and PDI of 130 ± 0.06 nm and 0.15 ± 0.004, respectively; and physical characterization of SL by DLS shows a good particle distribution (PDI 0.06 ± 0.001) with an average size of 140± 2.4 nm. The EE% of the BBH@NL and BBH@SL investigated by HPLC was 3.5 and 7%, respectively.

*3.2. Stability test*

The stability of the formulation was evaluated at two different temperatures (4, 25 °C) for up to 90 days. The formulation resulted stable at 4 °C meanwhile, a slight increase in size and PDI was seen after 90 days in the 25 °C condition. The amount of encapsulated drug was more stable at 4 °C and shows 1.04%, 1.26%, and 1,33% decrease in 7, 30, and 90 days. While more significant decrease in EE% has been seen in 25 °C which shows 1.08 %, 1.6%, and 2.38% decrease in 7, 30, and 90 days, respectively.

**Table 1.** Characterization of microfluidic liposomes. The decrease is announced based on the EE% at day zero. Data are reported as the mean of three independent replication of experiments ± SD.

| | 4 °C | | | 25 °C | | |
|---|---|---|---|---|---|---|
| Time (Days) | Size (nm) | PDI | EE% | Size (nm) | PDI | EE% |
| 7 | 141.2±0.01 | 0.06±0.01 | 1.04% ↓ | 140.1±6.1 | 0.06±0.01 | 1.08% ↓ |
| 14 | 139.75±0.45 | 0.059±0.004 | - | 141.6±0.2 | 0.053±0.01 | - |
| 30 | 144±1.3 | 0.056±0.001 | 1.26% ↓ | 151.35±1.05 | 0.058±0.002 | 1.6 % ↓ |
| 60 | 145.65±0.05 | 0.053±0.003 | - | 160.65±1.45 | 0.053±0.001 | - |
| 90 | 145.65±0.63 | 0.048±0.006 | 1.33% ↓ | 176.05±2.7 | 0.065±0.004 | 2.38% ↓ |

*3.3. Fourier-transform infrared spectroscopy (FTIR)*

FTIR analysis was carried out to evaluate the chemical structure of the microfluidic assembled liposomes (**Fig. 3**). In the spectrum of BBH@NL and BBH@SL, peaks at 1505 and 1331 $cm^{-1}$ are assigned to the presence of BBH in the BBH loaded liposome's structure. In addition, the peak at 1728 $cm^{-1}$ is related to the existence of SS in both SL and BBH@SL. In the liposome's spectrum, the peak at around 3342 $cm^{-1}$ is related to cholesterol with a slight shift to the right and a remarkable increase in intensity due to merging the characteristic peaks of cholesterol and the low-intensity peak of PC. The slight shift to the right might be evidence of the hydrophobic interaction and hydrogen bonding in the intermolecular structure of the liposomes (48). IR spectrum of BBH revealed an intense band at around 1003 $cm^{-1}$ and 1363 $cm^{-1}$, indicating the symmetric O-C-O stretch of the dioxolane ring and C-H group wag vibration in $C_6H_2$ and $C_5H_2$ rings (49). In the BBH spectrum, the band 2845 $cm^{-1}$ indicates alkane C–H stretching, and 1635 $cm^{-1}$ and 1331 $cm^{-1}$ refer to medium bending N-H and C-N in the amine group, respectively. The band at 1568 $cm^{-1}$ and 1505 $cm^{-1}$ show medium stretching C=C in cyclic alkene (50). In the spectrum of PC, the peaks at 2924 $cm^{-1}$ and 2854 $cm^{-1}$ are ascribed to C–H stretching group in the structure. The peaks around 1735 $cm^{-1}$, 1249 $cm^{-1}$, and 1173 $cm^{-1}$ are due to the stretching band of the ester carbonyl group, moderate stretching C-N amine band, and strong C-O stretching ester band, respectively (48). In the cholesterol spectrum, the characteristic peaks can be seen at 3405 $cm^{-1}$, 2866 $cm^{-1}$, 1466 $cm^{-1}$, 1376 $cm^{-1}$, and 1056 $cm^{-1}$ which refers to stretching hydroxyl group, symmetric

C-H stretching vibration, asymmetric stretching vibration of methylene and methyl group, bending vibration of methylene and methyl group and bending vibration of C-O group, respectively (34). The peak at 1728 $cm^{-1}$ shows the characteristic peak of SS (51) which is referred to a strong C=O band in an α,β-unsaturated ester.

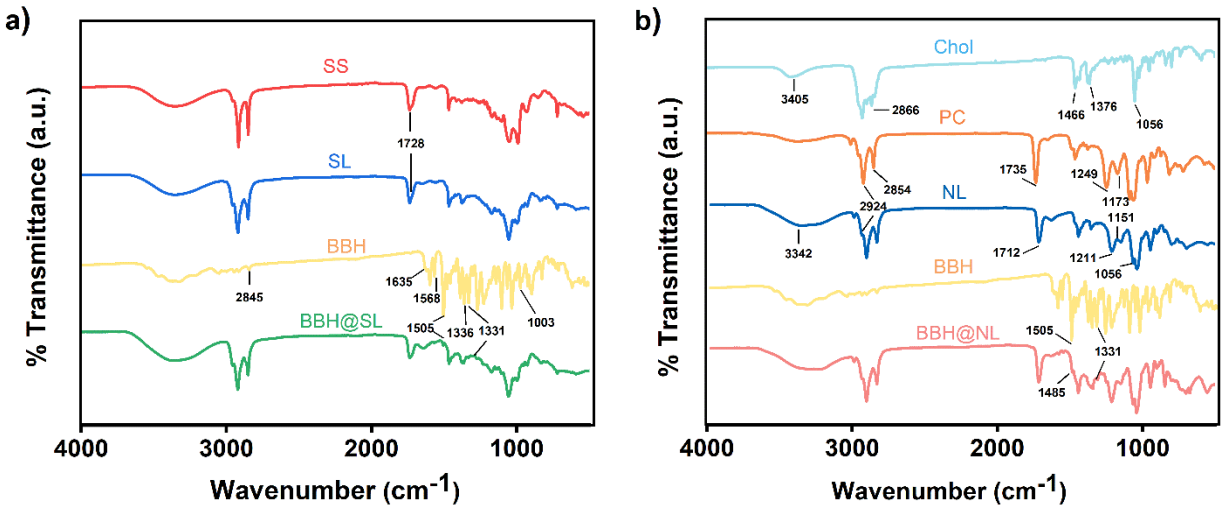


**Fig. 3.** Physicochemical characterization by FTIR analysis of a) BBH, SS, SL, and BBH@SL and b) BBH, PC, Chol, NL, BBH@NL demonstrated that interactions between components of NL and SL were able to slightly change the location of bands, indicating liposome formation.

### *3.4. Thermal gravimetric analysis (TGA) characterization*

Principal data on the composition of the liposomes, their water content, thermal stability, and their mass loss in specific temperatures (0- 500 °C) were obtained from TGA characterization. TGA curves showed the rates of water evaporation, water binding capacity, and stability of BBH, Chol, SS, PC, NL, BBH@NL, SL, BBH@SL (**Fig. 4 a, b**) (52). BBH presented thermal stability up to 350 °C showing a four-step degradation in the TGA curve from 350 to 500 °C confirming data reported in the literature (53). Sucrose ester's thermal behavior showed a broad step of mass loss decomposition, starting in the 100-250 °C range, which is ascribed to a random molecular decomposition (54). PC thermal degradation was found at approximately 97 °C and the TGA analyses of Cholesterol showed that the weight loss starts at 220-280 °C (55). The total weight loss of BBH, SS, PC, and Chol in thermal degradation was 44.8%, 96.4%, 94.9%, and 97.3%, respectively. The TGA graph of the NL and BBH@NL shows a thermal degradation refers to water loss starting at 100 °C and 5% of thermal degradation at 150 °C; on the contrary, no water loss occurred in SL and BBH@SL. The onset of initial

weight loss is around 256, 263, 218, 214 °C for NL, BBH@NL, SL, BBH@SL, respectively. The occurrence of the maximum degradation could be demonstrated from derivative thermogravimetry (DTG) analysis (**Fig. 4c**). The maximum degradation happens at <300 °C for the SL (253.4 °C and 296.3 °C for SL without and with BBH) and >300 °C for normal liposomes (341.65 °C and 332.9 °C for NL and BBH@NL, respectively). The residues in the NL and SL formulations are 5.15% and 6.14% of the initial weight, while the residue for the formulations containing the BBH is 10.17% and 17% for BBH@NL and BBH@SL, which refers to undegraded BBH in the formulation.

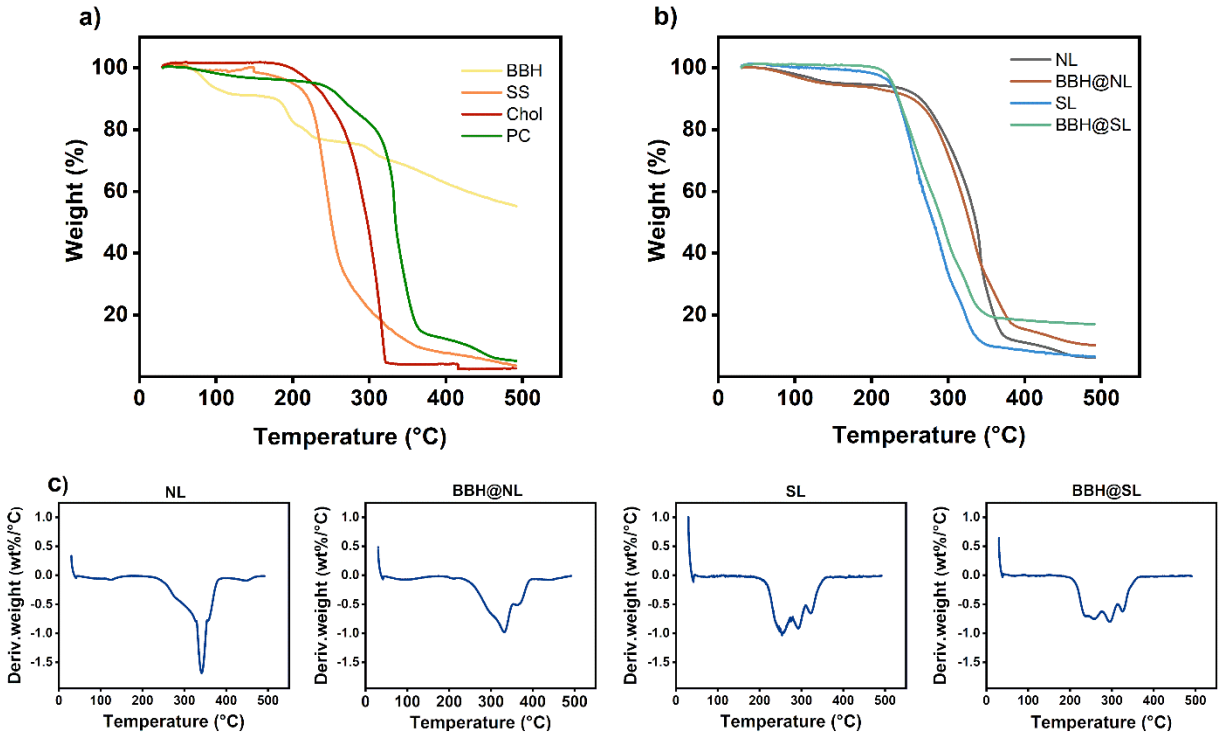


***F*ig. 4. a, b)** TGA (upper thermograms) **c)** and DTG (lower blue thermograms). The DTG thermograms are plotted for a better understanding of the rate of material weight changes upon heating up to 500 ºC.

## *3.5. Release studies*

### *3.5.1. In vitro release of berberine hydrochloride from liposomes*

The release profiles of BBH from BBH@SL and BBH@NL were studied at two different pH values of 7.4 and 5.5 to simulate physiologic and cancerous cells pH, respectively (40) (**Fig. 5 a, b**). The release

results in both mediums (acetate buffer and PBS) show that loading BBH into liposomes could decrease the release rate of the drug and provide a sustained release profile compared to free BBH solution. Moreover, BBH@SL showed faster drug release compared to BBH@NL due to the presence of SS, a permeability enhancer (56), which increases the liposome membrane permeability and drug release compared to the liposome without SS (0.23± 0.003 mg/mL, 0.2±0.007 mg/mL in BBH@SL and 0.14±0.004 mg/mL, 0.13±0.001 mg/mL in BBH@NL in acetate buffer and PBS, respectively).

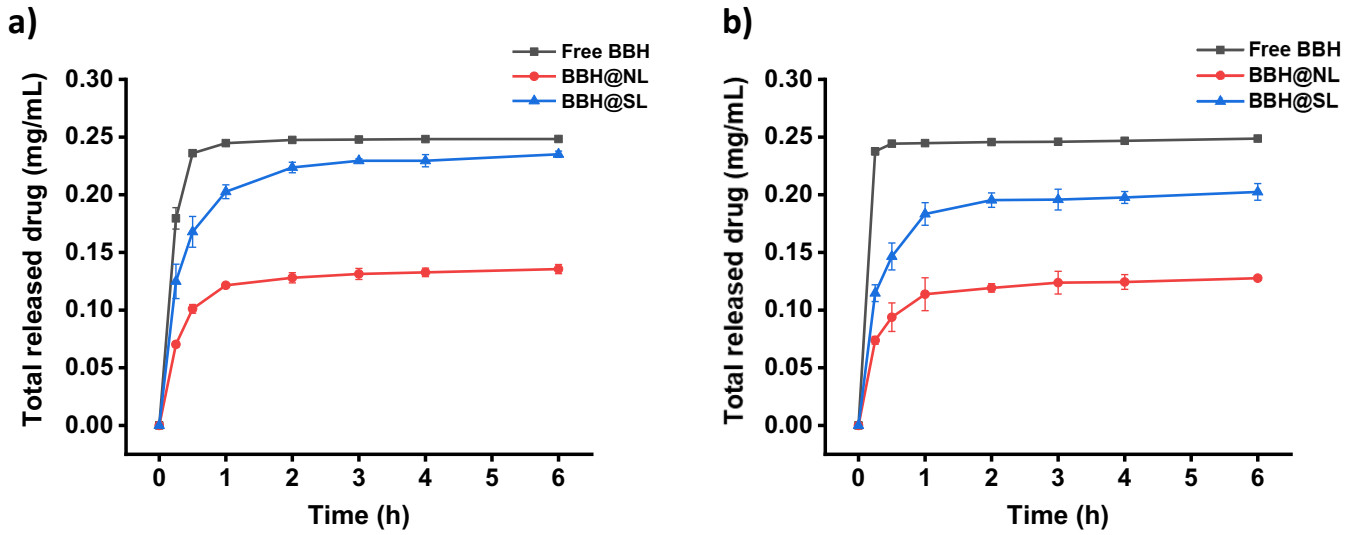


**Fig. 5.** BBH release from BBH@NL, BBH@SL and free BBH solution in a) acetate buffer (pH 5.5) b) PBS (pH 7.4) at 37 °C. Data are reported as the mean of three independent replication of experiments ± SD.

### *3.5.2. Mathematical Models of Releasing Kinetics*

The results obtained from the modeling of drug release profiles for each system evaluated at different environmental pH's, as well as their respective kinetic constants and adjusted-$R^2$ are shown in Table 2, where $k_1(h^{-1})$ is the first-order rate constant, $k_H(h^{-\frac{1}{2}})$ is the dissolution constant, $k_d(h^{-0,43})$ is the Fickian diffusional contribution and $k_s(h^{-0,43})$ the matrix swelling contribution (57).

**Table 2.** Kinetic constants are derived from the application of mathematical models to the drug release profiles.

| *Sample* | *Mathematical Model* | *Kinetic constants* | $R^2$ |
|---|---|---|---|
| *NL-Acetate buffer* | *First-order:* $M_t/M_0 = e^{-k_1 t}$ | $k_1 = 0.03 \pm 0.01 (h^{-1})$ | *0.33* |
| | *Higuchi:* $M_t/M_0 = k_H \sqrt[2]{t}$ | $k_H = 0.30 \pm 0.08\ (h^{-1})$ | *0.64* |
| | *Peppas-Salhin:* $M_t/M_0 = k_d \times t^m + k_s \times t^{2m}$ | $m = 0.43$<br>$k_d = 1.06 \pm 0.06\ (h^{-0.43})$<br>$k_s = -0.30 \pm 0.03\ (h^{-0.43})$ | *0.98* |
| *NL-PBS* | *First order:* $M_t/M_0 = e^{-k_1 t}$ | $k_1 = 0.03 \pm 0.01 (h^{-1})$ | *0.49* |
| | *Higuchi:* $M_t/M_0 = k_H \sqrt[2]{t}$ | $k_H = 0.3 \pm 0.1\ (h^{-1})$ | *0.66* |
| | *Peppas-Salhin:* $M_t/M_0 = k_d \times t^m + k_s \times t^{2m}$ | $m = 0.43$<br>$k_d = 0.99 \pm 0.01\ (h^{-0.43})$<br>$k_s = -0.3 \pm 0.3\ (h^{-0.43})$ | *0.97* |
| *SL-* acetate buffer | *First-order:* $M_t/M_0 = e^{-k_1 t}$ | $k_1 = 0.03 \pm 0.01 (h^{-1})$ | *0.45* |
| | *Higuchi:* $M_t/M_0 = k_H \sqrt[2]{t}$ | $k_H = 0.3 \pm 0.1\ (h^{-1})$ | *0.70* |
| | *Peppas-Salhin:* $M_t/M_0 = k_d \times t^m + k_s \times t^{2m}$ | $m = 0.43$<br>$k_d = 1.10 \pm 0.04\ (h^{-0.43})$<br>$k_s = -0.31 \pm 0.02\ (h^{-0.43})$ | *0.99* |
| *SL-PBS* | *First order:* $M_t/M_0 = e^{-k_1 t}$ | $k_1 = 0.03 \pm 0.01 (h^{-1})$ | *0.42* |
| | *Higuchi:* $M_t/M_0 = k_H \sqrt[2]{t}$ | $k_H = 0.3 \pm 0.1\ (h^{-1})$ | *0.66* |
| | *Peppas-Salhin:* $M_t/M_0 = k_d \times t^m + k_s \times t^{2m}$ | $m = 0.43$<br>$k_d = 1.06 \pm 0.04\ (h^{-0.43})$<br>$k_s = -0.31 \pm 0.02\ (h^{-0.43})$ | *0.98* |

The drug release profiles of all systems were better fitted by the Peppas-Salhin model as indicated by the $R^2$ values (**Table 2 and Fig. 6**). The Peppas-Salhin is a semiempirical model used to obtain information about the contributions of diffusion and matrix relaxation (or erosion) on drug release. The

coefficient m is the purely Fickian diffusion exponent related to a drug delivery system of any geometrical shape. As can be seen in Table 2, for all the systems, the $k_d$ kinetic constant is significantly higher than the $k_2$ kinetic constant, which, in turn, displayed a not significative negative value. This means that the drug release occurs by the Fickian diffusion mechanism without any contribution of the matrix swelling or erosion (58,59).

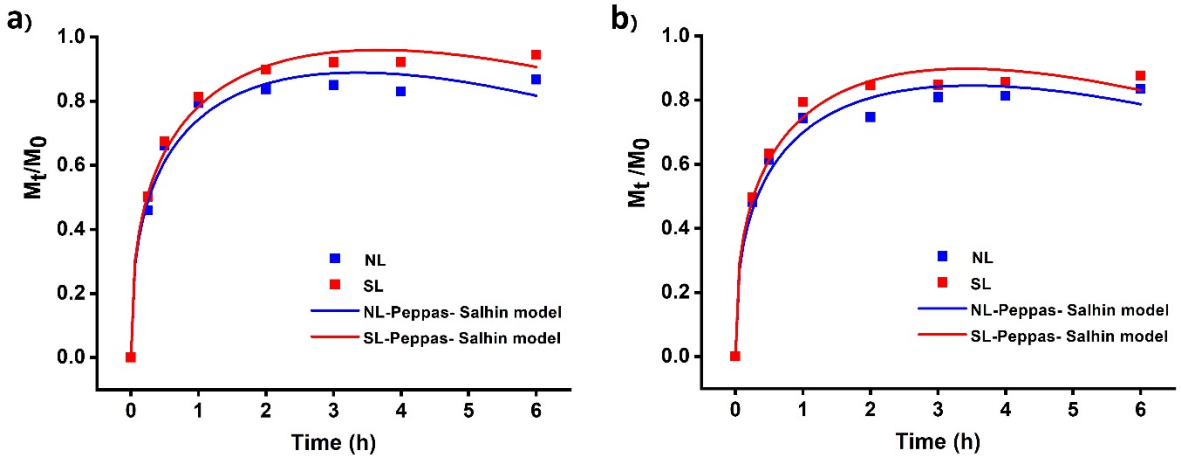


**Fig. 6.** Drug release profile of Free BBH, BBH@NL, and BBH@SL in a) acetate buffer b) PBS fitted by the Peppas-Salhin models.

### *3.6. In vitro cytocompatibility on Human Cardiomyocyte Cell Line (AC16)*

Cytotoxicity of the liposomes toward normal cardiomyocyte cells (AC16 cells) was evaluated by SRB assays (**Fig. 7**). No cytotoxic effects of NL and SL formulations were evident after 24 h treatment at all the concentrations tested. Only in the cases of free BBH (12 µg/mL) and BBH@SL (500 µg/mL) a statistically significant cell growth inhibition (up to 20 %) was observed by SRB test.

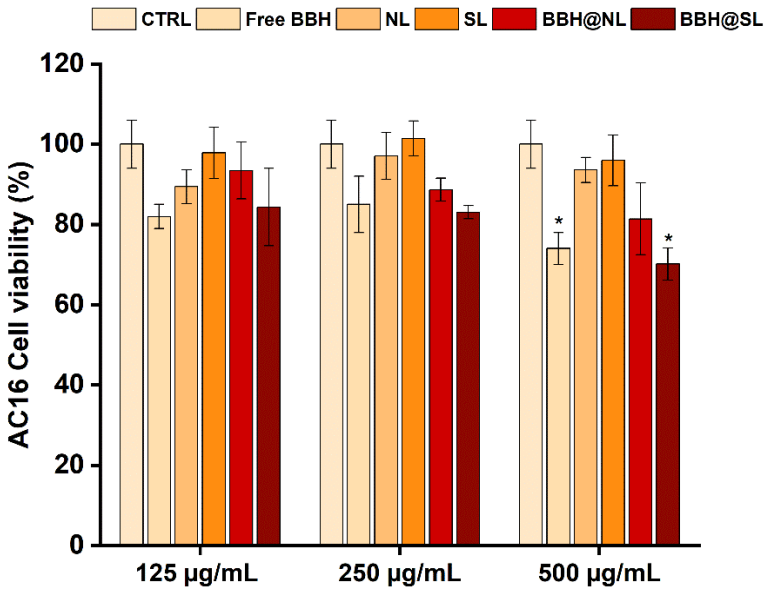


**Fig. 7.** AC16 cell growth (%) after 24 h treatment with NL, SL formulations (125, 250, 500 µg/mL) and free BBH (3, 6, 12 µg/mL) and BBH@NL and BBH@SL formulations 125, 250, 500 µg/mL (loaded with BBH 3, 6, 12 µg/mL). Cell viability was investigated using SRB test. Data are expressed as the mean± SD (n=3). *p<0.05 vs CTR (Tukey's test).

### *3.7. In vitro anti-proliferative test*

The anti-proliferative effect of the nanocarrier was determined by SRB assay (**Fig. 8**). Both SL and NL with and without BBH were studied to investigate if the presence of sucrose ester in the formulation could affect the antiproliferative activity on MDA-MB-231 cancer cells. Free BBH at the same concentration of the BBH loaded into liposomes was evaluated as a comparison. The SRB test demonstrates no cytotoxic effects of empty nanocarriers towards MDA-MB-231 after 24 h treatment. Free BBH did not show inhibition of cell growth in the range of concentrations tested (3-12 µg/mL comparable to the concentration of encapsulated BBH), in accordance with previous findings which demonstrated BBH cytotoxicity towards MDA-MB-231 cells only at very high doses (>20 µg/ml) (60). Significant cytotoxicity was observed in BBH@SL already at the concentration of 250 µg/mL (corresponding to 6 µg/mL loaded BBH) meanwhile, at the same concentration, BBH@NL did not show significant growth inhibition. Moreover, greater inhibition of cell growth was found by BBH@SL 500 µg/mL (-64 % vs. CTR) as compared to BBH@NL 500 µg/mL (-40 % vs, CTR). The difference between two formulations was statistically significant proving that the presence of the sugar moiety on

451 the surface of BBH@SL gives a positive effect on the efficacy of the sugar decorated nanocarrier
452 compared to the normal ones.

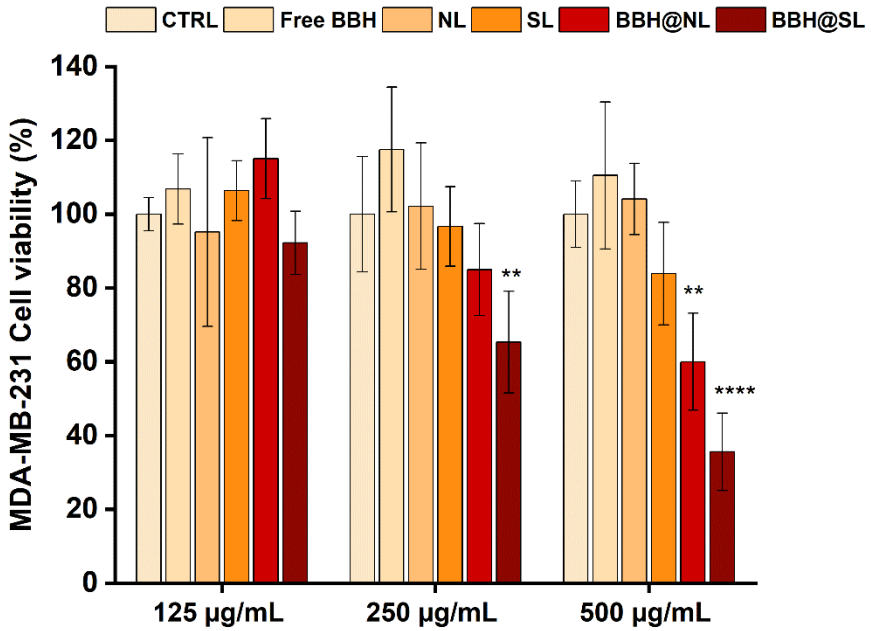


453 **Fig. 8.** MDA-MB-231 cell growth (%) after 24 h treatment with NL, SL formulations (125, 250, 500 µg/mL) and free BBH
454 (3, 6, 12 µg/mL corresponding to BBH loaded in SL) and BBH@NL and BBH@SL formulations 125, 250, 500 µg/mL.
455 Cell viability was investigated using the SRB test. Data are expressed as the mean± SD (n=3). **p<0.01, ****p<0.0001 vs
456 CTR and free BB (Tukey's test).
457

458 *3.8. Cell uptake studies*

459 The uptake of NL and SL by MDA-MB-231 breast cancer cells was analyzed by flow cytometry and
460 confocal microscopy after 4h (**Fig. 9**) and 24h (**Fig. 10**) to evaluate differences between the two
461 nanocarriers. In the MDA-MB-231 cell line tested after 4h, a well-detectable, bright fluorescence was
462 registered in SL samples (**Fig. 9a, c, e**) whereas in NL-treated cells only a negligible uptake was
463 detected, demonstrating that NL has a very slower uptake into the breast cancer cells compared to SL
464 which present the sugar moieties on the surface. The higher and, particularly, the faster liposome uptake
465 in SL formulation could explain the more efficient anti-proliferative activity of SL on MDA-MB-231
466 evaluated by the SRB assay.
467 To further investigate the mechanisms that drive these strong differences in the internalization of NL
468 and SL, we detected the expression of the transferrin receptor (CD71, normally involved in the iron
469 cellular uptake and strongly expressed on cells with a high proliferation rate (**Fig. 9b**).

Indeed, CD71 is a marker of poor prognosis in breast cancer and can predict response to Tamoxifen (61). We assessed the surface expression of CD71 on MDA-MB-231 cells, finding, in SL samples, moderate but significantly lower levels than control cells (**Fig. 9d**).

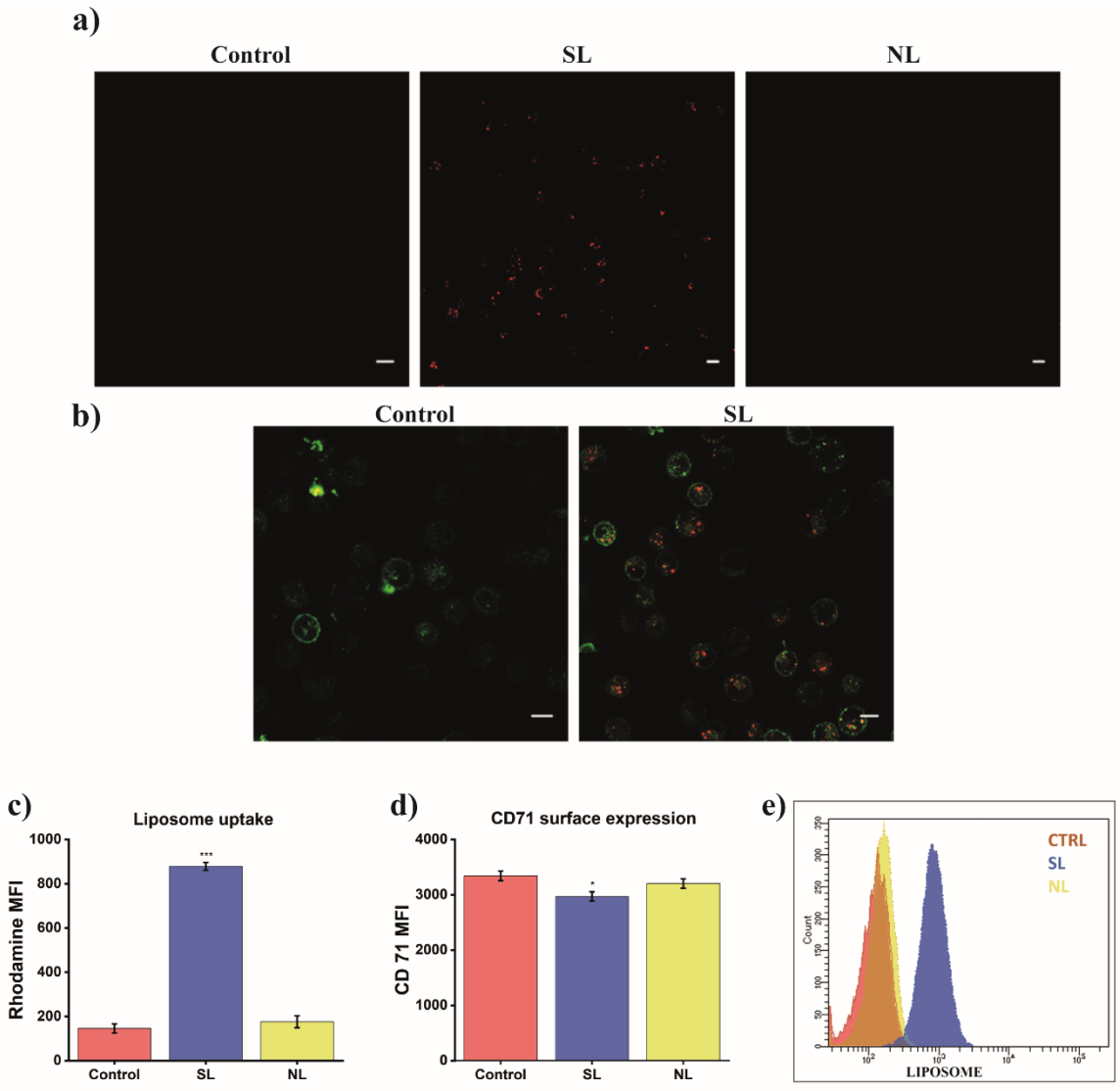


**Fig 9.** a) Single confocal optical section to evaluate liposome uptake (red) of SL treated MDA-MB-231 cells, after 4 h. b) Single confocal optical sections of liposome uptake (red) and CD71 (green) on MDA-MB-231 cells after 4 h. Scale bars 10 µm c) Statistical histogram of the liposome uptake after 4 h. Data are expressed as the mean± SD (n=3). ***p<0.0001 vs CTR and NL (Tukey's test). d) Statistical histogram of CD71 surface expression after 4 h. Data are expressed as the mean± SD (n=3). *p<0.01, vs CTR and NL (Tukey's test) e) Representative cytometric histogram of liposome internalization for Control, SL, and NL samples after 4 h.

CD71 also mediates the transport of IgA food complexes in epithelial cells (62) and, it may be involved in a specific binding (63). Of note, the moderate decrease of CD71 fluorescence observed in SL samples highlights a mild contribution of this surface molecule. We extended the analyses to 24 h after liposome administration. Confocal, flow cytometric, and statistic evaluations are shown in (**Fig. 10).**

Data highlight the extensive and significant uptake of NL, slightly greater than SL uptake (**Fig. 10 c, f**). In line with CD71 behavior observed for SL after 4 h, NL samples exhibit a mild decrease in CD71 expression (**Fig. 10 d**).

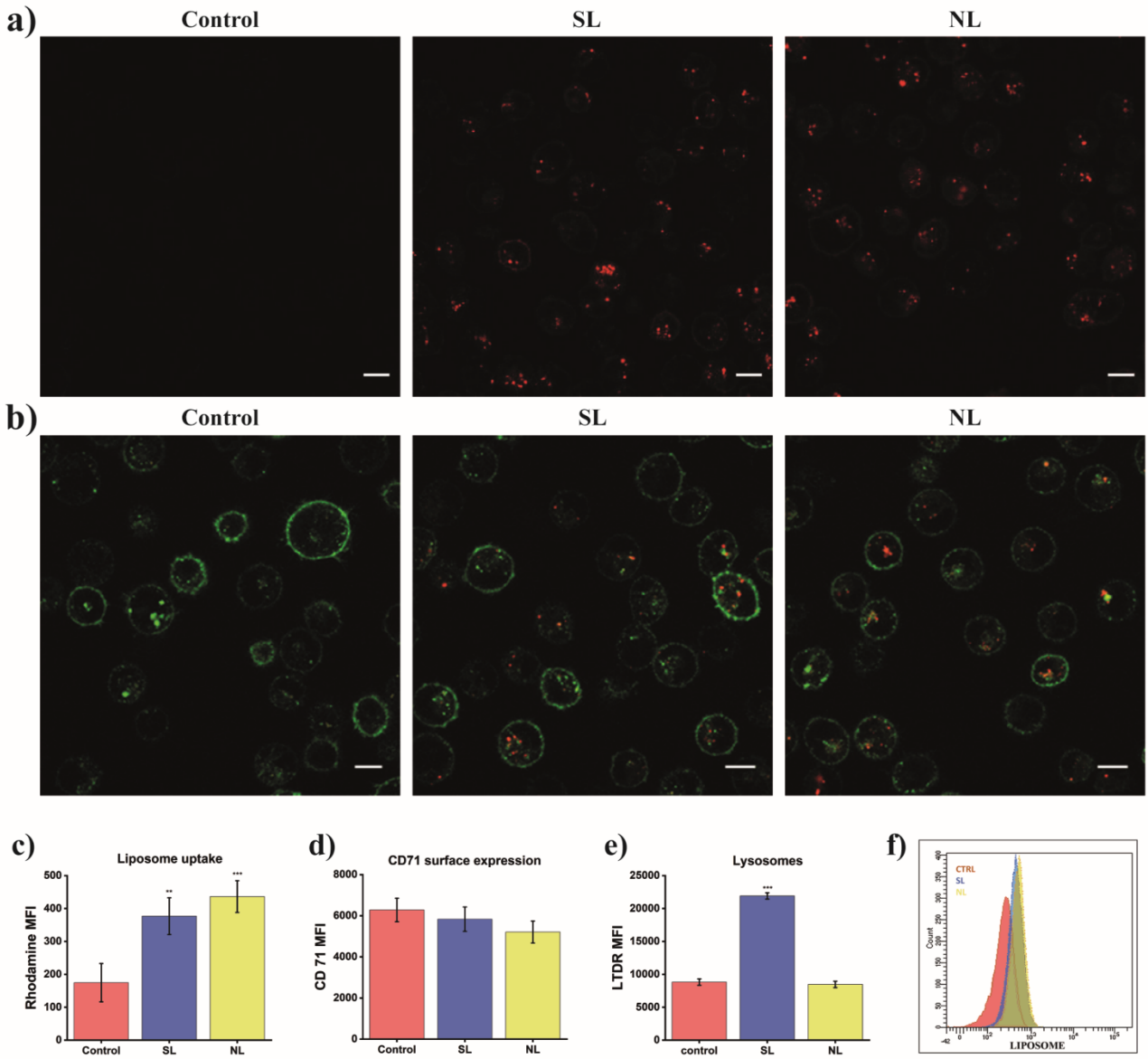


**Fig. 10** a) Single confocal optical section to evaluate liposome uptake (red) of SL treated MDA-MB-231 cells, after 24 h. b) Single confocal optical sections showing CD71 expression (green) and liposomes (red) on MDA-MB-231 cells after 24 h. Scale bars 10 µm. c) Statistical histogram of liposome uptake after 24 h. Data are expressed as the mean± SD (n=3).

**p<0.001, ***p<0.0001 vs CTR and NL (Tukey's test). d) Statistical histogram of CD71 after 24 h. e) Statistical histogram of LTDR MFI after 24 h. Data are expressed as the mean± SD (n=3). ***p<0.0001 vs CTR and NL (Tukey's test). f) Representative cytometric histogram of liposome internalization for Control, SL, and NL samples after 24 h.

Furthermore, to follow, at least in part, the intracellular journey of liposomes, we labeled breast cancer cells by the lysosomotropic probe LysoTracker Deep Red (LTG). Statistical and cytometric histograms are shown in (**Fig. 10 e)** and depict the increase of the number and functions of lysosomal structures and other acidic organelles (64). Furthermore, the confocal analysis highlights a co-localization of SL and acidic organelles (yellow spots) whereas no co-localized distribution is observable in NL treated cells.

These findings reveal profound differences also for the intracellular fate of the two different liposomal formulations, with a net SL tropism for lysosomal compartment, prospecting their possible use to target acidic vacuoles. Indeed, this peculiarity strengthens the evidence of the greater uptake of SL that, although degraded into lysosomes, reveal a similar NL fluorescence signal, after 24h, attesting a continuous, sustained SL uptake from the extracellular medium.

Finally, since cancer cells overexpress a wide variety of carbohydrate-binding receptors (3,4,36,65), including members of the C-type lectin receptor, Siglec (sialic acid-binding immunoglobulin-type lectin), galectin families (65), and the well-known CD206 receptor, highly expressed on MDA-MB-231 cells (66), sucrose receptor blocking study was performed.

To elucidate the capability to massively involve a varied pool of carbohydrate-binding receptors, a sucrose-cell pre-incubation was performed, as explained in Materials and Methods. The cellular uptake and its eventual sucrose-derived inhibition of SL were investigated after 20 and 40 minutes (**Fig. 11**). NL was not considered in this study since they did not show any uptake after 4h. A partial uptake inhibition was noticed after 20 minutes (around 20%) and after 40 minutes (around 30%) from starting the test. These results confirm that a sucrose-dependent uptake is present, but it is not the only one used to internalized the nanosized formulation.

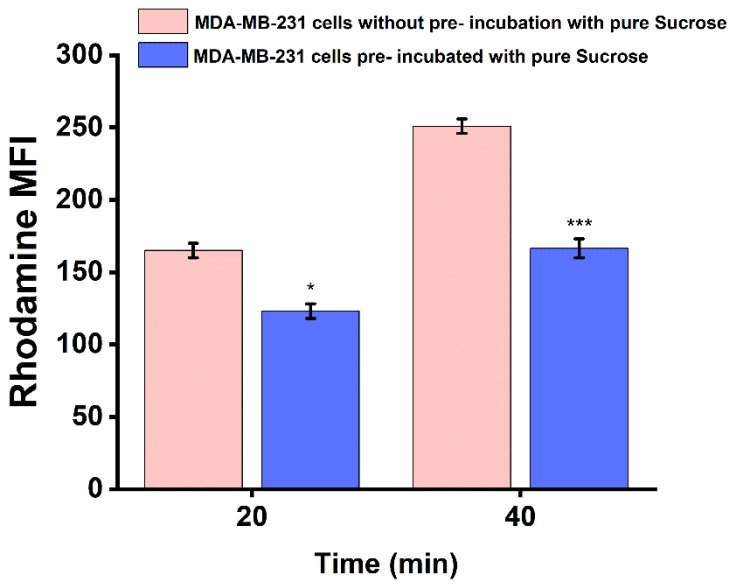


**Fig 11.** Statistical histogram of liposome uptake and its inhibition after 20' and 40' in normal-sized breast cancer cells, excluding cell debris. Data are expressed as the mean± SD (n=3). *p<0.01, ***p<0.0001 vs CTR and NL (Tukey's test).

## 4. Conclusions

In this work, we developed an innovative sugar-decorated colloidal drug delivery system assembled by 3D printed microfluidics. 3D printed microfluidics open the possibility to researchers to have easy access to this technology with the chance to personalize it based on their specific needs. Moreover, by employing the microfluidic method we have the potential to increase the liposomes preparation rate to enhance the very low conventional lab-scale rates. Our approach allows us to easily obtain stable and reproducible surface decorated delivery systems with no chemical steps needed before or after the production. The presence of the sugar moieties on the nanocarrier demonstrated an improvement of the cancer cell uptake resulting in an increased antiproliferative effect of the berberine-loaded sugar decorated liposomes. Taken together, this work demonstrates that, by microfluidic, it is possible to formulate drug-loaded sugar decorated liposomes with active targeting properties and tunable characteristics with an easy and scalable approach. Moreover, the proposed microfluidic assembled BBH@SL is a potential candidate as an antiproliferative carrier against triple-negative breast cancer cells.

**Acknowledgments**

The authors acknowledge ITIS E. Mattei (Urbino, PU, Italy) for the utilization of FTIR instrument

**Conflicts of interest:** The authors declare no conflict of interest

**CRediT authorship**

Shiva Khorshid: Methodology, Investigation, Data curation, Writing - original draft.

Mariele Montanari, Serena Benedetti, and Sofia Moroni: Methodology, Investigation, Data curation.

Annalisa Aluigi, Barbara Canonico and Stefano Papa: Methodology, Data curation, Writing - review & editing.

Mattia Tiboni: Conceptualization, Supervision, Methodology, Formal analysis, Data curation, Writing - review & editing

Luca Casettari: Conceptualization, Resources, Funding acquisition, Project administration, Supervision, Writing - review & editing.

**References**

1. WHO. Available from: https://www.who.int/news-room/fact-sheets/detail/breast-cancer

2. Guo Y, Pei X. Tetrandrine-Induced Autophagy in MDA-MB-231 Triple-Negative Breast Cancer Cell through the Inhibition of PI3K/AKT/mTOR Signaling. Evid Based Complement Alternat Med. 2019;2019:7517431.

3. Dalle Vedove E, Costabile G, Merkel OM. Mannose and Mannose-6-Phosphate Receptor–Targeted Drug Delivery Systems and Their Application in Cancer Therapy. Adv Healthc Mater [Internet]. 2018;7(14):1701398. Available from: https://onlinelibrary.wiley.com/doi/abs/10.1002/adhm.201701398

4. Ye Z, Zhang Q, Wang S, Bharate P, Varela-Aramburu S, Lu M, et al. Tumour-Targeted Drug Delivery with Mannose-Functionalized Nanoparticles Self-Assembled from Amphiphilic β-Cyclodextrins. Chem – A Eur J [Internet]. 2016;22(43):15216–21. Available from: https://chemistry-europe.onlinelibrary.wiley.com/doi/abs/10.1002/chem.201603294

5. Naeem S, Viswanathan G, Misran M. Liposomes as colloidal nanovehicles: On the road to success in intravenous drug delivery. Rev Chem Eng. 2017;34.

6. Wicki A, Witzigmann D, Balasubramanian V, Huwyler J. Nanomedicine in cancer therapy: challenges, opportunities, and clinical applications. J Control Release. 2015 Feb;200:138–57.

7. Sercombe L, Veerati T, Moheimani F, Wu SY, Sood AK, Hua S. Advances and Challenges of Liposome Assisted Drug Delivery. Front Pharmacol. 2015;6:286.

8. Shepherd SJ, Issadore D, Mitchell MJ. Microfluidic formulation of nanoparticles for biomedical applications. Biomaterials [Internet]. 2021;274:120826. Available from: https://www.sciencedirect.com/science/article/pii/S0142961221001824

9. Tiboni M, Tiboni M, Pierro A, Del Papa M, Sparaventi S, Cespi M, et al. Microfluidics for nanomedicines manufacturing: An affordable and low-cost 3D printing approach. Int J Pharm [Internet]. 2021;599:120464. Available from: https://www.sciencedirect.com/science/article/pii/S0378517321002696

10. Costa C, Liu Z, Simões SI, Correia A, Rahikkala A, Seitsonen J, et al. One-step microfluidics production of enzyme-loaded liposomes for the treatment of inflammatory diseases. Colloids Surfaces B Biointerfaces [Internet]. 2021;199:111556. Available from: https://www.sciencedirect.com/science/article/pii/S0927776520309139

11. Liu H, Singh RP, Zhang Z, Han X, Liu Y, Hu L. Microfluidic Assembly: An Innovative Tool for the Encapsulation, Protection, and Controlled Release of Nutraceuticals. J Agric Food Chem [Internet]. 2021 Mar 17;69(10):2936–49. Available from: https://doi.org/10.1021/acs.jafc.0c05395

12. Kotouček J, Hubatka F, Mašek J, Kulich P, Velínská K, Bezděková J, et al. Preparation of nanoliposomes by microfluidic mixing in herring-bone channel and the role of membrane fluidity in liposomes formation. Sci Rep [Internet]. 2020;10(1):5595. Available from: https://doi.org/10.1038/s41598-020-62500-2

13. Aghaei H, Solaimany Nazar AR, Varshosaz J. Double flow focusing microfluidic-assisted based preparation of Methotrexate–Loaded liposomal nanoparticles: Encapsulation efficacy, drug release and stability. Colloids Surfaces A Physicochem Eng Asp. 2021;614:126166.

14. Mancera-Andrade1 EI, Parsaeimehr1 A, Arevalo-Gallegos1 A, AscencioFavela1 G, , Roberto Parra-Saldivar1, 2, 3 4. Microfluidics technology for drug delivery: A review. 2018;

15. Grycová L, Dostál J, Marek R. Quaternary protoberberine alkaloids. Phytochemistry [Internet]. 2007;68(2):150–75. Available from: https://www.sciencedirect.com/science/article/pii/S0031942206006261

16. Küpeli E, Koşar M, Yeşilada E, Hüsnü K, Başer C. A comparative study on the anti-inflammatory, antinociceptive and antipyretic effects of isoquinoline alkaloids from the roots of Turkish Berberis species. Life Sci. 2002 Dec;72(6):645–57.

17. Kuo C-L, Chi C-W, Liu T-Y. The anti-inflammatory potential of berberine in vitro and in vivo. Cancer Lett [Internet]. 2004;203(2):127–37. Available from: https://www.sciencedirect.com/science/article/pii/S0304383503005949

18. Yeşilada E, Küpeli E. Berberis crataegina DC. root exhibits potent anti-inflammatory, analgesic and febrifuge effects in mice and rats. J Ethnopharmacol. 2002 Feb;79(2):237–48.

19. Cernáková M, Kostálová D. Antimicrobial activity of berberine--a constituent of Mahonia aquifolium. Folia Microbiol (Praha). 2002;47(4):375–8.

20. Pierpaoli E, Cirioni O, Simonetti O, Orlando F, Giacometti A, Lombardi P, et al. Potential application of berberine in the treatment of Escherichia coli sepsis. Nat Prod Res. 2020 Feb;1–6.

21. Zhang X, Sun X, Wu J, Wu Y, Wang Y, Hu X, et al. Berberine Damages the Cell Surface of Methicillin-Resistant Staphylococcus aureus. Front Microbiol [Internet]. 2020;11:621. Available from: https://www.frontiersin.org/article/10.3389/fmicb.2020.00621

22. Meeran SM, Katiyar S, Katiyar SK. Berberine-induced apoptosis in human prostate cancer cells is initiated by reactive oxygen species generation. Toxicol Appl Pharmacol. 2008 May;229(1):33–43.

23. Mantena SK, Sharma SD, Katiyar SK. Berberine, a natural product, induces G1-phase cell cycle arrest and caspase-3-dependent apoptosis in human prostate carcinoma cells. Mol Cancer Ther. 2006 Feb;5(2):296–308.

24. Wang L, Liu L, Shi Y, Cao H, Chaturvedi R, Calcutt MW, et al. Berberine Induces Caspase-Independent Cell Death in Colon Tumor Cells through Activation of Apoptosis-Inducing Factor. PLoS One [Internet]. 2012;7(5):1–12. Available from: https://doi.org/10.1371/journal.pone.0036418

25. Hsu W-H, Hsieh Y-S, Kuo H-C, Teng C-Y, Huang H-I, Wang C-J, et al. Berberine induces apoptosis in SW620 human colonic carcinoma cells through generation of reactive oxygen species and activation of JNK/p38 MAPK and FasL. Arch Toxicol. 2007 Oct;81(10):719–28.

26. Piyanuch R, Sukhthankar M, Wandee G, Baek SJ. Berberine, a natural isoquinoline alkaloid, induces NAG-1 and ATF3 expression in human colorectal cancer cells. Cancer Lett. 2007 Dec;258(2):230–40.

27. Patil JB, Kim J, Jayaprakasha GK. Berberine induces apoptosis in breast cancer cells (MCF-7) through mitochondrial-dependent pathway. Eur J Pharmacol [Internet]. 2010;645(1):70–8. Available from: https://www.sciencedirect.com/science/article/pii/S0014299910007569

28. Mantena SK, Sharma SD, Katiyar SK. Berberine inhibits growth, induces G1 arrest and apoptosis in human epidermoid carcinoma A431 cells by regulating Cdki-Cdk-cyclin cascade, disruption of mitochondrial membrane potential and cleavage of caspase 3 and PARP. Carcinogenesis. 2006 Oct;27(10):2018–27.

29. Kong W, Wei J, Abidi P, Lin M, Inaba S, Li C, et al. Berberine is a novel cholesterol-lowering drug working through a unique mechanism distinct from statins. Nat Med. 2004 Dec;10(12):1344–51.

30. Pierpaoli E, Arcamone AG, Buzzetti F, Lombardi P, Salvatore C, Provinciali M. Antitumor effect of novel berberine derivatives in breast cancer cells. BioFactors [Internet]. 2013;39(6):672–9. Available from: https://iubmb.onlinelibrary.wiley.com/doi/abs/10.1002/biof.1131

31. Bhowmik D, Buzzetti F, Fiorillo G, Orzi F, Syeda TM, Lombardi P, et al. Synthesis of new 13-diphenylalkyl analogues of berberine and elucidation of their base pair specificity and energetics of DNA binding. Med Chem Commun [Internet]. 2014;5(2):226–31. Available from: http://dx.doi.org/10.1039/C3MD00254C

32. Cui H-X, Hu Y-N, Li J-W, Yuan K, Guo Y. Preparation and Evaluation of Antidiabetic Agents of Berberine Organic Acid Salts for Enhancing the Bioavailability. Molecules. 2018 Dec;24(1).

33. Tiboni M, Benedetti S, Skouras A, Curzi G, Perinelli DR, Palmieri GF, et al. 3D-printed microfluidic chip for the preparation of glycyrrhetinic acid-loaded ethanolic liposomes. Int J Pharm [Internet]. 2020;584:119436. Available from: https://www.sciencedirect.com/science/article/pii/S0378517320304208

34. Elmowafy E, El-Derany MO, Biondo F, Tiboni M, Casettari L, Soliman ME. Quercetin Loaded Monolaurate Sugar Esters-Based Niosomes: Sustained Release and Mutual Antioxidant—Hepatoprotective Interplay. Pharmaceutics [Internet]. 2020;12(2). Available from: https://www.mdpi.com/1999-4923/12/2/143

35. Moisés Blanco Calvo,1 Angélica Figueroa,1 Enrique Grande Pulido,2 Rosario García Campelo 3 and Luís Antón Aparicio. Potential Role of Sugar Transporters in Cancer and Their Relationship with Anticancer Therapy. 2010;

36. Ahire JH, Behray M, Webster CA, Wang Q, Sherwood V, Saengkrit N, et al. Synthesis of Carbohydrate Capped Silicon Nanoparticles and their Reduced Cytotoxicity, In Vivo Toxicity, and Cellular Uptake. Adv Healthc Mater. 2015 Aug;4(12):1877–86.

37. Calvo MB, Figueroa A, Pulido EG, Campelo RG, Aparicio LA. Potential Role of Sugar Transporters in Cancer and Their Relationship with Anticancer Therapy. Naor Z, editor. Int J Endocrinol [Internet]. 2010;2010:205357. Available from: https://doi.org/10.1155/2010/205357

38. Kikkeri R, Lepenies B, Adibekian A, Laurino P, Seeberger PH. In Vitro Imaging and in Vivo Liver Targeting with Carbohydrate Capped Quantum Dots. J Am Chem Soc [Internet]. 2009 Feb 18;131(6):2110–2. Available from: https://doi.org/10.1021/ja807711w

39. Lim Y, Lee M. Self-assembled multivalent carbohydrate ligands. Org Biomol Chem [Internet]. 2007;5(3):401–5. Available from: http://dx.doi.org/10.1039/B615744K

40. Abazari R, Ataei F, Morsali A, Slawin AMZ, L. Carpenter-Warren C. A Luminescent Amine-Functionalized Metal–Organic Framework Conjugated with Folic Acid as a Targeted Biocompatible pH-Responsive Nanocarrier for Apoptosis Induction in Breast Cancer Cells. ACS Appl Mater Interfaces [Internet]. 2019 Dec 11;11(49):45442–54. Available from:

https://doi.org/10.1021/acsami.9b16473

41. Benedetti S, Catalani S, Canonico B, Nasoni MG, Luchetti F, Papa S, et al. The effects of Acyclovir administration to NCI-H1975 non-small cell lung cancer cells. Toxicol Vitr [Internet]. 2022;79:105301. Available from: https://www.sciencedirect.com/science/article/pii/S0887233321002265

42. Brad Chazotte. Labeling Lysosomes in Live Cells with LysoTracker. 2010;

43. Canonico B, Cesarini E, Salucci S, Luchetti F, Falcieri E, Di Sario G, et al. Defective Autophagy, Mitochondrial Clearance and Lipophagy in Niemann-Pick Type B Lymphocytes. PLoS One [Internet]. 2016;11(10):1–31. Available from: https://doi.org/10.1371/journal.pone.0165780

44. Habashy HO, Powe DG, Staka CM, Rakha EA, Ball G, Green AR, et al. Transferrin receptor (CD71) is a marker of poor prognosis in breast cancer and can predict response to tamoxifen. Breast Cancer Res Treat [Internet]. 2009;119(2):283. Available from: https://doi.org/10.1007/s10549-009-0345-x

45. Le NT V, Richardson DR. The role of iron in cell cycle progression and the proliferation of neoplastic cells. Biochim Biophys Acta. 2002 Oct;1603(1):31–46.

46. Sorvillo N, Pos W, van den Berg LM, Fijnheer R, Martinez-Pomares L, Geijtenbeek TB, et al. The macrophage mannose receptor promotes uptake of ADAMTS13 by dendritic cells. Blood [Internet]. 2012;119(16):3828–35. Available from: https://doi.org/10.1182/blood-2011-09-377754

47. Zhang W, Coughlin ML, Metzger JM, Hackel BJ, Bates FS, Lodge TP. Influence of Cholesterol and Bilayer Curvature on the Interaction of PPO–PEO Block Copolymers with Liposomes. Langmuir [Internet]. 2019 Jun 4;35(22):7231–41. Available from: https://doi.org/10.1021/acs.langmuir.9b00572

48. Salama A, Badran M, Elmowafy M, Soliman GM. Spironolactone-Loaded LeciPlexes as Potential Topical Delivery Systems for Female Acne: In Vitro Appraisal and Ex Vivo Skin Permeability Studies. Pharmaceutics. 2019 Dec;12(1).

49. Leona M, Lombardi J. Identification of berberine in ancient and historical textiles by surface-enhanced Raman scattering. J Raman Spectrosc. 2007;38:853–8.

50. Battu SK, Repka MA, Maddineni S, Chittiboyina AG, Avery MA, Majumdar S. Physicochemical characterization of berberine chloride: a perspective in the development of a solution dosage form for oral delivery. AAPS PharmSciTech. 2010 Sep;11(3):1466–75.

51. Csizmazia E, Eros G, Berkesi O, Berkó S, Szabó-Révész P, Csányi E. Ibuprofen penetration enhance by sucrose ester examined by ATR-FTIR in vivo. Pharm Dev Technol. 2012;17(1):125–8.

52. Kwon SS, Kong BJ, Park SN. Physicochemical properties of pH-sensitive hydrogels based on hydroxyethyl cellulose–hyaluronic acid and for applications as transdermal delivery systems for skin lesions. Eur J Pharm Biopharm. 2015;92:146–54.

53. Dahryn Trivedi1, Mahendra Kumar Trivedi1, Alice Branton1, Gopal Nayak1 and SJ. Consciousness Energy Healing Treatment Influenced the Physicochemical and Thermal Properties of Berberine Chloride. JSM Anal Bioanal Tech. 2019;

54. Pan X, Sengupta P, Webster DC. Novel biobased epoxy compounds: epoxidized sucrose esters of fatty acids. Green Chem [Internet]. 2011;13(4):965–75. Available from: http://dx.doi.org/10.1039/C0GC00882F

55. Dave V, Gupta A, Singh P, Gupta C, Sadhu V, Reddy KR. Synthesis and characterization of celecoxib loaded PEGylated liposome nanoparticles for biomedical applications. Nano-Structures & Nano-Objects [Internet]. 2019;18:100288. Available from: https://www.sciencedirect.com/science/article/pii/S2352507X19300010

56. El-Laithy HM, Shoukry O, Mahran LG. Novel sugar esters proniosomes for transdermal delivery of vinpocetine: Preclinical and clinical studies. Eur J Pharm Biopharm [Internet]. 2011;77(1):43–55. Available from: https://www.sciencedirect.com/science/article/pii/S0939641110002857

57. Malekjani N, Jafari SM. Modeling the release of food bioactive ingredients from carriers/nanocarriers by the empirical, semiempirical, and mechanistic models. Compr Rev Food Sci Food Saf [Internet]. 2021;20(1):3–47. Available from: https://ift.onlinelibrary.wiley.com/doi/abs/10.1111/1541-4337.12660

58. Bruschi ML, editor. 5 - Mathematical models of drug release. In: Strategies to Modify the Drug

Release from Pharmaceutical Systems [Internet]. Woodhead Publishing; 2015. p. 63–86. Available from: https://www.sciencedirect.com/science/article/pii/B9780081000922000059

59. Peppas NA, Sahlin JJ. A simple equation for the description of solute release. III. Coupling of diffusion and relaxation. Int J Pharm [Internet]. 1989;57(2):169–72. Available from: https://www.sciencedirect.com/science/article/pii/0378517389903062

60. Yao M, Fan X, Yuan B, Takagi N, Liu S, Han X, et al. Berberine inhibits NLRP3 Inflammasome pathway in human triple-negative breast cancer MDA-MB-231 cell. BMC Complement Altern Med [Internet]. 2019;19(1):216. Available from: https://doi.org/10.1186/s12906-019-2615-4

61. Mitsis1 M, Alexiou2 GA, Vartholomatos2 E, Markopoulos3 G, Lazari4 D, , Entela Hodaj4, 5 DN, et al. N-(p-coumaroyl) serotonin induces cell cycle arrest and apoptosis in breast cancer cells. 2018;

62. Ménard S, Cerf-Bensussan N, Heyman M. Multiple facets of intestinal permeability and epithelial handling of dietary antigens. Mucosal Immunol [Internet]. 2010;3(3):247–59. Available from: https://doi.org/10.1038/mi.2010.5

63. Sun L-X, Lin Z-B, Duan X-S, Lu J, Ge Z-H, Li M, et al. Ganoderma lucidum polysaccharides counteract inhibition on CD71 and FasL expression by culture supernatant of B16F10 cells upon lymphocyte activation. Exp Ther Med [Internet]. 2013;5(4):1117–22. Available from: https://doi.org/10.3892/etm.2013.931

64. Bik E, Mateuszuk L, Orleanska J, Baranska M, Chlopicki S, Majzner K. Chloroquine-Induced Accumulation of Autophagosomes and Lipids in the Endothelium. Int J Mol Sci [Internet]. 2021;22(5). Available from: https://www.mdpi.com/1422-0067/22/5/2401

65. Anderluh M, Berti F, Bzducha-Wróbel A, Chiodo F, Colombo C, Compostella F, et al. Emerging glyco-based strategies to steer immune responses. FEBS J [Internet]. 2021;288(16):4746–72. Available from: https://febs.onlinelibrary.wiley.com/doi/abs/10.1111/febs.15830

66. Grugan KD, McCabe FL, Kinder M, Greenplate AR, Harman BC, Ekert JE, et al. Tumor-Associated Macrophages Promote Invasion while Retaining Fc-Dependent Anti-Tumor Function. J Immunol [Internet]. 2012;189(11):5457–66. Available from: https://www.jimmunol.org/content/189/11/5457

758